Computing Ship Wave Resistance from Wave Amplitude with a Non-local Absorbing Boundary Condition (submitted for publication to Communications in Numerical Methods in Engineering)

by M. Storti, J. D'Elía and S. Idelsohn

Grupo de Tecnología Mecánica del INTEC
Güemes 3450, 3000 - Santa Fe, Argentina
Phone/Fax: 54-42-55.91.75, Fax: 54-42-55.09.44
e-mail: mstorti@minerva.unl.edu.ar
home-page: http://venus.unl.edu.ar/gtm-eng.html

File:

$Id: wdrag12.tex,v 6.11 1997/12/16 15:16:11 mstorti Exp $

Subject Classification:

- 76B20 Ship waves / Incompressible inviscid fluids, potential theory / Fluid mechanics
- 65N30 Finite elements, Rayleigh-Ritz and Galerkin methods, finite methods / Partial differential equations, boundary value problems / Numerical analysis

Summary

A method for computing ship wave resistance from a momentum flux balance is presented. It is based on computing the momentum flux carried by the gravity waves that exit the computational domain through the outlet plane. It can be shown that this method ensures a non-negative wave resistance, in contrast with straightforward integration of the normal pressure forces. However, this calculation should be performed on a transverse plane located far behind the ship. Traditional Dawson-like methods add a numerical viscosity that dampens the wave pattern so that some amount of momentum flux is lost, and resulting in an error in the momentum balance. The flow field is computed, then, with a centered scheme with absorbing boundary conditions[1].

Keywords

- potential flow
- finite element method
- wave resistance
- absorbing boundary condition
- free surface flow
- partial discretization

Table of Contents

1. Introduction
2. Governing equations
3. Wave resistance from wave amplitude
4. Numerical implementation
4.1. Partial discretization
4.2. The DNL absorbing boundary condition
4.3. Discrete expression for the momentum flux
5. Numerical examples
5.1. Submerged dipole
5.2. Parabolic pressure distribution
5.3. Wigley hull
5.4. Rectangular pressure distribution
6. Conclusions
7. Acknowledgments
8. References

1. Introduction

When a body moves near the free surface of a fluid, a pattern of trailing gravity waves is formed. The energy spent in building this pattern comes from the work done by the body against the *wave resistance*. Numerical modeling of this problem is a matter of high interest for ship design, and marine engineering[2–10]. As a first approximation, the wave resistance can be computed with a potential model, whereas for the viscous drag it can be assumed that the position of the surface is held fixed at the reference hydrostatic position, i.e. a plane. This is, basically, the *Froude's hypotheses*[7].

We concentrate in this paper in the computation of the flow field and wave resistance for a body in steady motion, by means of a potential model for the fluid and a linearized free surface boundary condition. This is the basis for most ship design codes in industry. The governing equations are the Laplace equation with slip boundary conditions on the hull and channel walls, inlet/outlet conditions at the corresponding planes and the free surface boundary condition. The free surface boundary condition amounts to a Neumann boundary condition with a source term proportional to the streamlined second derivative of the potential. However, the problem as stated so far is ill posed, in the sense that it is invariant under longitudinal coordinate inversion ($x \to -x$), and it is clear then, that it can not capture the characteristic trailing waves propagating downstream. To do this, we can either add a dissipative numerical mechanism or impose some kind of *"absorbing boundary condition"* at the outlet boundary.

Usually the wave resistance is computed from straightforward integration of the pressure forces over the hull. However, it is well known that this can give negative wave resistance, which is physically incorrect[4]. Even for potential flow without free surface pressure integration yields non-zero (either positive or negative) drag, whereas it is well known that in such situation the drag should be null. This non-physical drag is caused by incorrect integration of the pressure forces, specially in regions with strong variations as near the nose in airfoils.

Alternatively, the wave resistance can be computed from the downstream wave pattern by means of a momentum flux balance. In order to ensure a correct evaluation, this computation should be performed in a plane located far downstream from the ship. However, traditional Dawson-like methods are dissipative and some amount of momentum is lost, introducing an error in the computation. Notwithstanding the fact that upwind or numerical viscosity methods are today a well established technique[11–13], it is evident the interest in finding a method that do not lean on such additives. In another paper[1], we presented a method which is based on an absorbing boundary condition at the outlet plane so that no numerical viscosity is needed. The discrete wave pattern has no damping, allowing the computation of force by means of the proposed momentum flux balance. In this work, we show in detail this computation.

2. Governing equations

Consider the flow around a ship moving at constant speed in a channel of constant section which, for simplicity, is assumed to be a rectangle of depth H and width L_y as shown in figure 1. The fluid to be modeled occupies region Ω

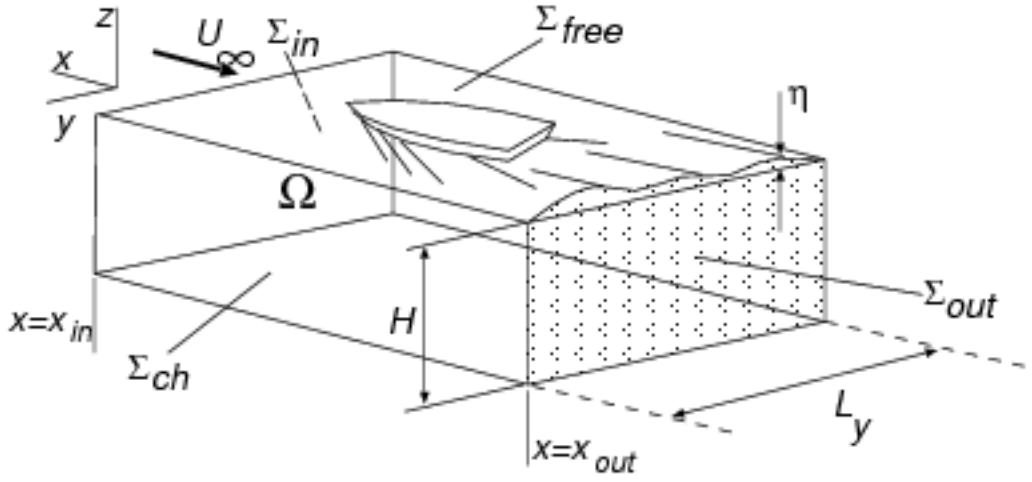

Figure 1: Geometrical description. (File: gxeplit)

which is bounded by: the channel walls and bottom Σ_{ch}, the inlet/outlet boundaries $\Sigma_{\text{in/out}}$, the wetted surface of the ship Σ_{ship} and the free surface Σ_{free}. The governing equations are:

$$\begin{aligned}
&\Delta\Phi = 0 && \text{for } \mathbf{x} \text{ in } \Omega \\
&\Phi_{,n} = 0 && \text{at } \Sigma_{\text{free}} + \Sigma_{\text{ch}} + \Sigma_{\text{ship}} \\
&\tfrac{1}{2}|\nabla\Phi|^2 + g\eta = \tfrac{1}{2}{U_\infty}^2 && \text{at } \Sigma_{\text{free}} \\
&\Phi = U_\infty x && \text{at } \Sigma_{\text{in}} \\
&\text{radiation b.c.'s} && \text{at } \Sigma_{\text{out}}
\end{aligned} \qquad \text{(1.a-e)}$$

The Laplace equation (1.a) comes from the assumption that the flow is irrotational and incompressible. The usual slip condition (1.b) is imposed at the channel walls, bottom and free surface. Equation (1.c) is the *"free surface boundary condition"*. It comes from the Bernoulli equation (including a hydrostatic term gz, η stands for the surface elevation) and it is usually linearized under certain assumptions as, for instance, that the ship is either thin, slender, slow or deeply submerged[4]. The *"radiation boundary conditions"* should allow, roughly speaking, the flow of energy in the form of radiating waves to propagate downstream and exit cleanly at Σ_{out}. In contrast, no waves are allowed to propagate upstream to Σ_{in} so that we simply impose that the potential should approach the undisturbed one there. Note that, the different treatment in Σ_{in} and Σ_{out} is the only element that can break the symmetry $x \to -x$, and ensure a physically correct wave pattern. Another mean of doing this is the addition of some *"upwind"* or *"numerical dissipation"* mechanism.

In slow ship theory, the flow is decomposed in a base flow Φ_0, also called *"double body flow"*, and a *"wave perturbation"* flow[4] ϕ:

$$\Phi = \Phi_0 + \phi \qquad (2)$$

The great simplification comes from the fact that the governing equations for both flows are restricted to the domain Ω_0 where the free surface Σ_{free} has been

replaced by the undisturbed position of the free surface $\Sigma_{\text{free}\,0}$, which in this case is simply the plane $z = 0$. The double body flow satisfies the Laplace equation with slip boundary condition on the undisturbed free surface. As the undisturbed free surface is a plane, it acts as a mirror and the problem is equivalent to an exterior flow around a closed body formed by reflecting (*"doubling"*) the hull about the undisturbed free surface. In addition, far (downstream or upstream) from the ship the double body flow approaches uniform flow $\Phi_0 = U_\infty x$. With all these assumptions, the linearized governing equations for ϕ are [2,4,6–7],

$$\left|\begin{array}{lll} \Delta\phi = 0, & \text{in} & \Omega_0 \\ \phi_{,n} = 0, & \text{at} & \Sigma_{\text{ch}} \\ \phi = 0, & \text{at} & \Sigma_{\text{in}} \\ \phi_{,n} + K^{-1}\,\phi_{,xx} = 0, & \text{at} & \Sigma_{\text{free}} \\ \text{radiation b.c.'s}, & \text{at} & \Sigma_{\text{out}} \end{array}\right. \tag{3.a-e}$$

where $K = g/{U_\infty}^2$ is the *characteristic wave number* of the flow.

3. Wave resistance from wave amplitude

Usually, the drag on the ship is obtained by integration of the normal pressure forces over the ship:

$$F_x = \int_{\Sigma_{\text{ship}}+\Sigma_{\text{ship,upper}}} p\, n_x \; dS \tag{4}$$

Pressure comes from the Bernoulli's equation:

$$p + \tfrac{1}{2}\rho(\nabla\phi)^2 + \rho g z = p_\infty + \tfrac{1}{2}\rho {U_\infty}^2 \tag{5}$$

from which (1.c) is simply the particularization at the free surface. We will start from these expressions to find an expression involving the state of the fluid at the outlet plane only. The pressure is constant on the non-wetted part of the ship $\Sigma_{\text{ship,upper}}$, and, as the ship is a closed surface:

$$\begin{aligned} F_x &= \int_{\Sigma_{\text{ship}}+\Sigma_{\text{ship,upper}}} p\, n_x \; dS - \int_{\Sigma_{\text{ship}}+\Sigma_{\text{ship,upper}}} p_\infty\, n_x \; dS \\ &= \int_{\Sigma_{\text{ship}}} (p - p_\infty)\, n_x \; dS \end{aligned} \tag{6}$$

Since the surface $\Sigma_{\text{in/out}}+\Sigma_{\text{ch}}+\Sigma_{\text{free}}+\Sigma_{\text{ship}}$ is closed (it is the boundary of domain Ω):

$$\begin{aligned} \int_{\Sigma_{\text{in/out}}+\Sigma_{\text{ch}}+\Sigma_{\text{free}}+\Sigma_{\text{ship}}} & [(p - p_\infty)\hat{\mathbf{e}}_x] \cdot \hat{\mathbf{n}} \; dS = \\ &= \int_\Omega \nabla \cdot [(p - p_\infty)\hat{\mathbf{e}}_x] \; d\Omega \\ &= \int_\Omega \frac{\partial p}{\partial x} \; d\Omega \end{aligned} \tag{7}$$

where $\hat{\mathbf{e}}_x$ is a unit vector in the x direction and $\hat{\mathbf{n}}$ a normal unit vector exterior to Ω. But $\hat{\mathbf{e}}_x \cdot \hat{\mathbf{n}} = 0$ at Σ_{ch} (since the channel has constant section) and $p = p_\infty$ at Σ_{free} and then:

$$F_x = -\int_{\Sigma_{\text{in/out}}} (p - p_\infty)\, n_x \; dS + \int_\Omega \frac{\partial p}{\partial x} \; d\Omega \tag{8}$$

From the Bernoulli equation and using the irrotationality of the velocity vector $\mathbf{U} = \nabla\Phi$ and the continuity equation:

$$\begin{aligned} \frac{\partial p}{\partial x} &= \frac{\partial}{\partial x}[p_\infty + \tfrac{1}{2}\rho({U_\infty}^2 - U^2) - \rho g z] \\ &= -\rho U_i \frac{\partial U_i}{\partial x} \\ &= -\rho U_i \frac{\partial U_x}{\partial x_i} \\ &= -\rho \frac{\partial}{\partial x_i}(U_i U_x) \\ &= -\rho \nabla \cdot (U_x \, \mathbf{U}) \end{aligned} \tag{9}$$

and:

$$\begin{aligned} \int_\Omega \frac{\partial p}{\partial x} \; d\Omega &= -\rho \int_\Omega \nabla \cdot (U_x \, \mathbf{U}) \; d\Omega \\ &= -\rho \int_{\Sigma_{\text{in/out}}+\Sigma_{\text{ch}}+\Sigma_{\text{free}}+\Sigma_{\text{ship}}} U_x \, \mathbf{U} \cdot \hat{\mathbf{n}} \; dS \\ &= -\rho \int_{\Sigma_{\text{in/out}}} U_x^2 \; dS \end{aligned} \tag{10}$$

Replacing in (8):

$$F_x = G(x_{\text{in}}) - G(x_{\text{out}}) \tag{11}$$

where $G(x)$ is the momentum flux through the surface at a plane $x = \text{cnst}$.

$$G(x) = \int_{\Sigma_x} (p - p_\infty + \rho U_x^2) \; dz \; dy \tag{12}$$

note that (11) is valid for any x_{in} as long as it is located before the hull, but, as the drag force must not depend on x_{in}, that means that $G(x)$ must be of the form shown in figure 2, it has some variation in that part of the x axis occupied by the hull and is constant in the remaining part. The wave resistance F_x amounts to the difference between this constant values.

These expressions have been derived for the non-linear system (1) and we have to find the appropriated expressions for the linearized form (3). Far from the ship, we can assume that $\Phi_0 = U_\infty x$ and then, using Bernoulli's equation and neglecting terms higher than quadratic in the perturbation potential ϕ:

$$G(x) = \int_{\Sigma_x} \{\tfrac{1}{2}\rho[2U_\infty(U_\infty + \phi_{,x}) + \phi_{,x}^2 - \phi_{,y}^2 - \phi_{,z}^2)] - \rho g z\} \; dS \tag{13}$$

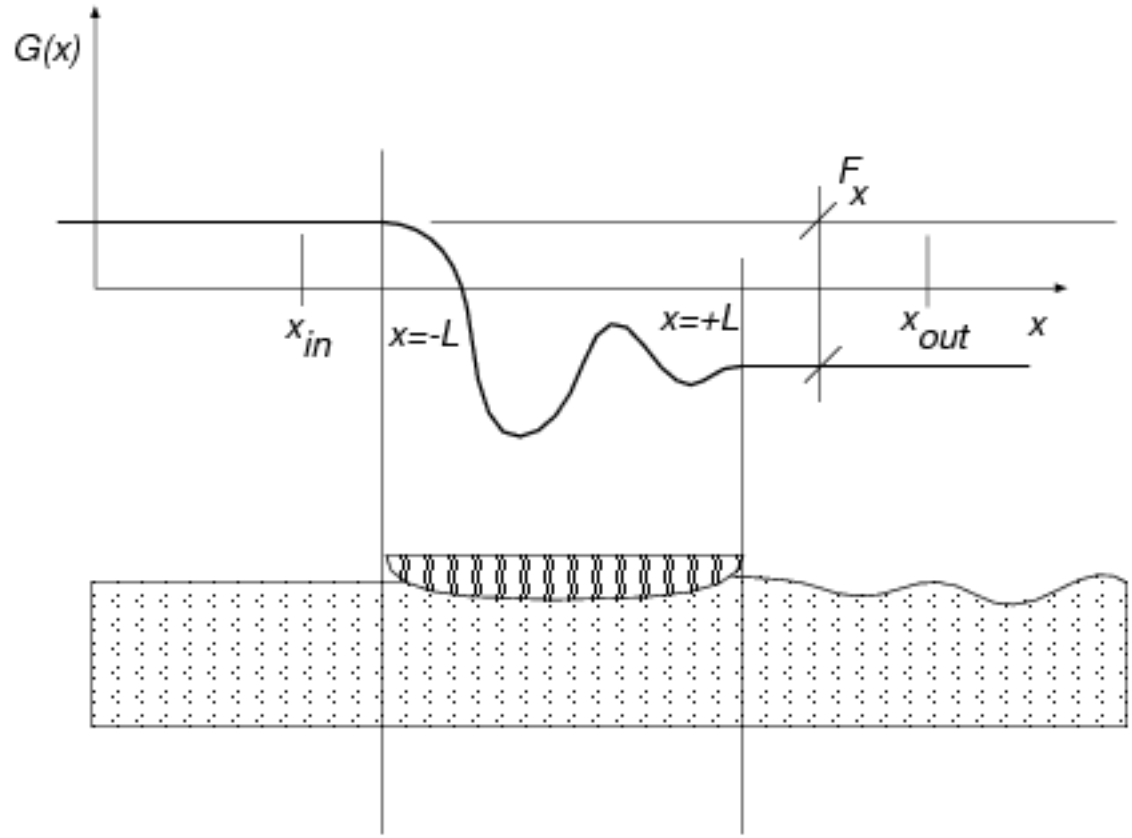

Figure 2: Momentum flux G as function of the longitudinal coordinate x.(Fig. gx)

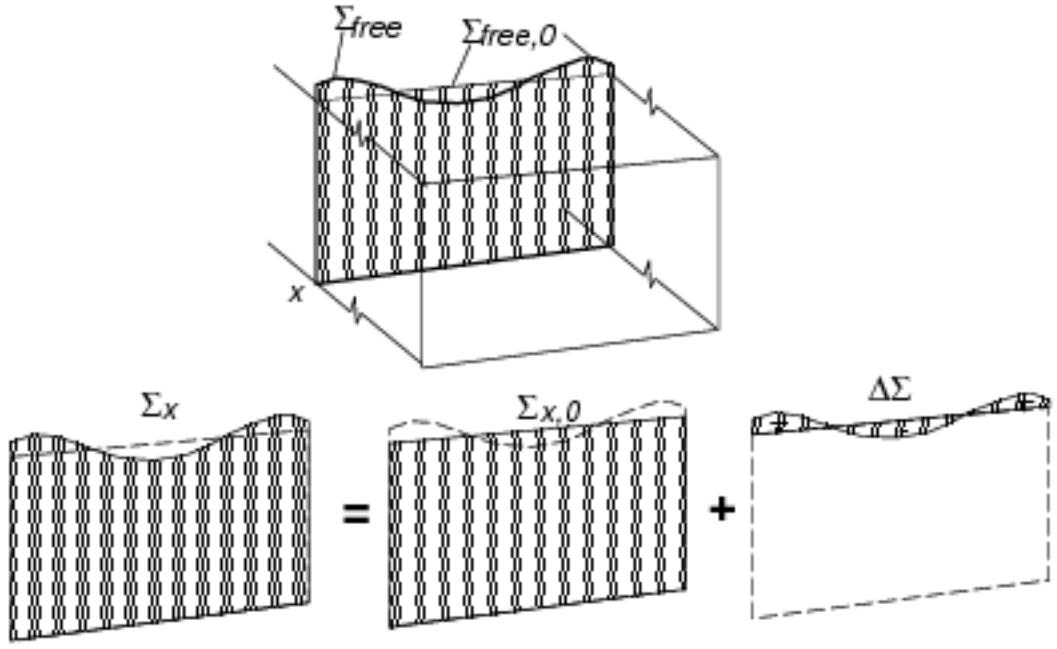

Figure 3: The actual section Σ_x is the sum of the non-perturbed section $\Sigma_{x,0}$ and the "section change" $\Delta\Sigma$.(Fig. dsigma)

Now consider the contribution from the term:

$$\rho U_\infty \int_{\Sigma_x} U_x \; dS = U_\infty \dot{M} = \text{cte} \tag{14}$$

Which is constant for all x ($\dot{M}$ is the mass flow through Σ_x). But a constant is irrelevant in $G(x)$ since the wave resistance comes from a difference (see equation (11)). The same is true for the contribution of the hydrostatic pressure from the non perturbed channel section $\Sigma_{x,0}$ (see figure 3), and the contribution from the rest $\Delta\Sigma = \Sigma_x - \Sigma_{x,0}$ can be explicitly calculated as:

$$\int_{y=-L_y/2}^{+L_y/2} \int_{z=0}^{\eta} z \; dz \; dy = \int_{y=-L_y/2}^{+L_y/2} \tfrac{1}{2}\eta^2 \; dy \tag{15}$$

Finally, as ϕ and η are of the same order, we can neglect the contribution from $\phi_{,x}^2 - \phi_{,y}^2 - \phi_{,z}^2$ over $\Delta\Sigma$ in (13). The appropriated linearized expression is then:

$$G(x) = \tfrac{1}{2}\rho \int_{\Sigma_{x,0}} (u_x^2 - u_y^2 - u_z^2) \; dS - \tfrac{1}{2}\rho g \int_{y=-L_y/2}^{+L_y/2} \eta^2 \; dy \tag{16}$$

4. Numerical implementation

We will recall how the linearized system is solved with the DNL(from *Discrete Non-Local*) absorbing boundary conditions and, then, we will see how expression (16) is computed. Details on the DNL can be found in a companion paper[1].

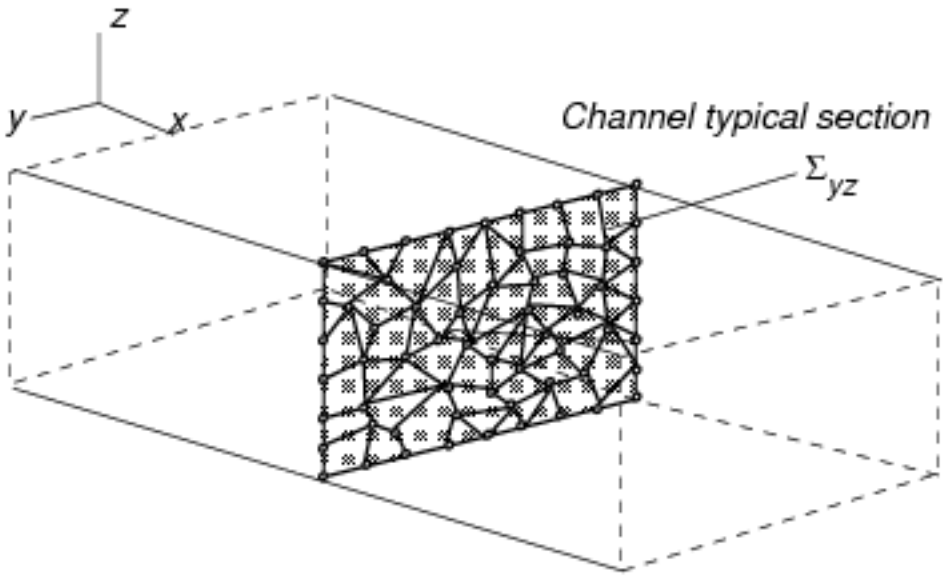

Figure 4: Partial discretization of the problem in yz. FEM unstructured mesh on the typical channel section.(File: typsect)

4.1. Partial discretization: We will assume a FEM partial discretization of this PDE in the transversal (y) and depth (z) directions in the far downstream and upstream regions $|x| > L$. This is done by defining a FEM mesh on the channel typical section (see figure 4), and replacing:

$$\phi(x,y,z) \sim \hat{\phi}(x,y,z) = \sum_{k=1}^{N_{\text{slab}}} \phi_k(x)\, N_k(y,z) \tag{17}$$

where N_{slab} is the number of nodes in the typical section, and $N_k(y,z)$ the two-dimensional interpolation functions. Replacing this in the Laplace equation(3.a), integrating by parts and using the free surface boundary condition, the following system of ODE's is obtained:

$$\bar{\mathbf{M}}\,\boldsymbol{\phi}_{,xx} - \mathbf{K}\boldsymbol{\phi} = \mathbf{0} \tag{18}$$

where:

$$\begin{aligned}
\boldsymbol{\phi}(x) &= \begin{bmatrix} \phi_1(x) \\ \phi_2(x) \\ \vdots \\ \phi_{N_{\text{slab}}}(x) \end{bmatrix} \\
K_{jk} &= \int_{\Sigma_{\text{x,0}}} \nabla_{yz} N_j(y,z) \cdot \nabla_{yz} N_k(y,z)\; dy\; dz \\
\bar{\mathbf{M}} &= \mathbf{M} - K^{-1}\mathbf{M}_{\text{free}} \\
M_{jk} &= \int_{\Sigma_{\text{x,0}}} N_j(y,z)\, N_k(y,z)\; dy\; dz \\
M_{\text{free},jk} &= \int_{\Sigma_{\text{free o}}} N_j(y,z)\, N_k(y,z)\; dy
\end{aligned} \tag{19.a-e}$$

$\boldsymbol{\phi}(x)$ is the vector of nodal potentials and $\mathbf{M}$ and $\mathbf{K}$ are the typical FEM matrices for the identity (mass matrix) and Laplace operators. The modified mass matrix $\bar{\mathbf{M}}$ includes the *"free surface mass matrix"* $\mathbf{M}_{\text{free}}$. $\mathbf{M}$ and $\mathbf{M}_{\text{free}}$ are positive definite mass matrices, $\mathbf{K}$ is positive semi-definite and all of them are symmetric. Due to the negative sign in (19.c) $\bar{\mathbf{M}}$ *has not a definite sign.*

4.2. The DNL absorbing boundary condition:

System (18) is decoupled in a series of scalar ODE's if we make the change of basis $\mathbf{U} = \mathbf{S}^{-1}\boldsymbol{\phi}$, where $\mathbf{S}$ solves the following eigenvalue problem:

$$\mathbf{K}\mathbf{S} = \bar{\mathbf{M}}\mathbf{S}\boldsymbol{\Lambda} \tag{20}$$

with $\boldsymbol{\Lambda}$ a diagonal matrix. We denote by $\boldsymbol{\phi}_k$ the k-th column of $\boldsymbol{\Lambda}$, i.e. the k-th eigenvector and by $\lambda_k = \boldsymbol{\Lambda}_{kk}$ the corresponding eigenvalue. Due to the properties of $\bar{\mathbf{M}}$ and $\mathbf{K}$ ($\mathbf{K}$ is symmetric positive definite and $\bar{\mathbf{M}}$ is symmetric) it can be shown that such decomposition is possible and $\mathbf{S}$ and $\boldsymbol{\Lambda}$ are real. We assume that

the eigenvalues are sorted in ascending order. $\boldsymbol{\Lambda}$ has in general a certain number of negative eigenvalues that, we will see later, are responsible of the wave resistance:

$$\begin{cases} \lambda_k < 0; & \text{for } 1 \le k \le N_{\text{inv}} \text{ (inviscid modes)} \\ \lambda_k > 0; & \text{for } N_{\text{inv}}+1 \le k \le N_{\text{slab}} \text{ (pure viscous modes)} \end{cases} \tag{21}$$

In addition, as is usual for this kind of eigenvalue problems, the eigenvectors are orthogonal with respect to both $\tilde{\mathbf{M}}$ and $\mathbf{K}$, i.e.:

$$\boldsymbol{\phi}_k^T \cdot \tilde{\mathbf{M}} \boldsymbol{\phi}_j = 0, \quad \boldsymbol{\phi}_k^T \cdot \mathbf{K} \boldsymbol{\phi}_j = 0, \quad \text{if } j \neq k \tag{22}$$

The equation for each component U_k of $\mathbf{U}$ is:

$$U_{k,xx} - \lambda_k U_k = 0 \tag{23}$$

and its general solution is:

$$U_k(x) = \begin{cases} b_k^+ e^{+i\mu_k x} + b_k^- e^{-i\mu_k x} & ; \text{for } 1 \le k \le N_{\text{inv}} \\ a_k^+ \, e^{+\mu_k x} + a_k^- \, e^{-\mu_k x} & ; \text{for } N_{\text{inv}}+1 \le k \le N_{\text{slab}} \end{cases} \tag{24}$$

where $\mu_k = \sqrt{|\lambda_k|}$. In order to have a bounded solution we must have $a_k^+ = 0$ for $x > L$ and $a_k^- = 0$ for $x < -L$ for the pure viscous modes and, then:

$$\left.\begin{array}{ll} U_{k,x} + \mu_k \, U_k = 0, & \text{at } x = x_{\text{out}} \\ U_{k,x} - \mu_k \, U_k = 0, & \text{at } x = x_{\text{in}} \end{array}\right\} \quad k = N_{\text{inv}}+1, \ldots, N_{\text{slab}} \tag{25}$$

These are the appropriated absorbing boundary conditions for the pure viscous modes. The same criteria can not be applied to the inviscid modes, since they do not grow or decay for $x \to \pm\infty$. However a detailed physical analysis shows that viscous dissipation tends to shift the pure imaginary eigenvalues towards the $\text{Re}\{z\} < 0$ semi-plane. This means that $b_k^{\pm} = 0$ for $x < 0$ and, then, the appropriated boundary condition is:

$$U_k = U_{k,x} = 0 \qquad \text{at } x = x_{\text{in}}, \; k = N_{\text{inv}}+1, \ldots, N_{\text{slab}} \tag{26}$$

Equations (25,26) represent a set of $2N_{\text{slab}}$ boundary conditions that close the system of governing equations (18). Absorbing boundary conditions are well known in the context of other wave-like phenomena like the Helmholtz equations[14–21], but are seldom used in the ship wave resistance problem due to inherent dificulties in developping such conditions. Lenoir & Tounsi[17] addressed the problem of absorbing boundary conditions for the sea-keeping problem, which is more closely related to the Helmholtz problem than to the wave-resistance problem. The boundary conditions presented here for the wave resistance problem are completely absorbent, in the sense that the solution is independent of the position of the boundary where it is imposed. They are *nonlocal* in the sense that, in the $\boldsymbol{\phi}$ basis, they represent full matrices connecting all the unknowns at two consecutive layers at the inlet and outlet planes.

For a rectangular cross section channel, the eigenvalue decomposition for the continuum problem may be solved in closed form, as described in the work of Patlashenko & Givoli[21] (see also Givoli et.al.[20]). However, for several reasons, we consider that it is preferable to solve the eigenvalue problem at the discrete level. First, if the eigenvalue problem is solved at the continuum level, then there are an infinite number of eigenvalues, and the series must be truncated somewhere. If not enough terms are added, then the boundary condition would have some amount of reflection. In contrast, the discrete eigenvalue problem alternative, is "parameter free" in this sense, and gives absolutely no reflection. In addition, the discrete version may easily include an arbitrary cross channel section (this may be useful for certain experimental configurations) and boundary conditions at the walls and bottom.

The extension to the full discrete problem (i.e., discretized also in the x direction) is straightforward. However, a detailed discussion is found in a companion paper[1].

The far field expressions are:

$$\boldsymbol{\phi}(x) = \begin{cases} \displaystyle\sum_{k=N_{\text{inv}}+1}^{N_{\text{slab}}} a_k^+ \, e^{\mu_k x} \boldsymbol{\phi}_k & ; \text{ for } x < -L \\ \displaystyle\sum_{k=1}^{N_{\text{inv}}} b_k \sin(\mu_k x + \gamma_k) \boldsymbol{\phi}_k + \sum_{k=N_{\text{inv}}+1}^{N_{\text{slab}}} a_k^- \, e^{-\mu_k x} \boldsymbol{\phi}_k & ; \text{ for } x > L \end{cases} \tag{27}$$

where the imaginary exponentials have been brought, by convenience, to trigonometric form.

4.3. Discrete expression for the momentum flux:

We now apply (16) to the partially discrete solution of (18,25,26). From (17):

$$\begin{aligned} u_x &= \frac{\partial \phi}{\partial x} = \sum_{k=1}^{N_{\text{slab}}} \dot{\phi}_k \, N_k(y,z) \\ u_y &= \frac{\partial \phi}{\partial y} = \sum_{k=1}^{N_{\text{slab}}} \phi_k \, \frac{\partial}{\partial y} N_k(y,z) \\ u_z &= \frac{\partial \phi}{\partial z} = \sum_{k=1}^{N_{\text{slab}}} \phi_k \, \frac{\partial}{\partial z} N_k(y,z) \end{aligned} \tag{28}$$

Here the dotts means partial differentiation with respect to x. We can compute

each of the terms in (16):

$$\begin{aligned}
\int_{\Sigma_{\mathrm{x},0}} u_x^2 \, dy \, dz &= \int_{\Sigma_{\mathrm{x},0}} \frac{\partial \phi}{\partial x} \frac{\partial \phi}{\partial x} \, dy \, dz \\
&= \int_{\Sigma_{\mathrm{x},0}} \left[\sum_{j=1}^{N_{\mathrm{slab}}} \dot{\phi}_j \, N_j(y,z) \right] \left[\sum_{k=1}^{N_{\mathrm{slab}}} \dot{\phi}_k \, N_k(y,z) \right] dy \, dz \\
&= \sum_{j,k=1}^{N_{\mathrm{slab}}} \dot{\phi}_j \, \dot{\phi}_k \int_{\Sigma_{\mathrm{x},0}} [N_j(y,z) \, N_k y, z) \, dy \, dz] \\
&= \sum_{j,k=1}^{N_{\mathrm{slab}}} M_{jk} \, \dot{\phi}_j \, \dot{\phi}_k \\
&= \dot{\boldsymbol{\phi}}^T \cdot \mathbf{M} \, \dot{\boldsymbol{\phi}}
\end{aligned} \tag{29}$$

$$\begin{aligned}
&\int_{\Sigma_{\mathrm{x},0}} (u_y^2 + u_z^2) \, dy \, dz = \\
&\quad = \int_{\Sigma_{\mathrm{x},0}} (\nabla_{yz} \phi) \cdot (\nabla_{yz} \phi) \, dy \, dz \\
&\quad = \int_{\Sigma_{\mathrm{x},0}} \left[\sum_{j=1}^{N_{\mathrm{slab}}} \phi_j \, \nabla_{yz} N_j(y,z) \right] \cdot \left[\sum_{k=1}^{N_{\mathrm{slab}}} \phi_k \, \nabla_{yz} N_k(y,z) \right] dy \, dz \\
&\quad = \sum_{j,k=1}^{N_{\mathrm{slab}}} \phi_j \, \phi_k \int_{\Sigma_{\mathrm{x},0}} [\nabla_{yz} N_j(y,z)] \cdot [\nabla_{yz} N_k(y,z)] \, dy \, dz \\
&\quad = \boldsymbol{\phi}^T \cdot \mathbf{K} \, \boldsymbol{\phi}
\end{aligned} \tag{30}$$

$$\begin{aligned}
\int_{y=-L_y/2}^{+L_y/2} \eta^2 \, dy &= (U_\infty/g)^2 \int_{y=-L_y/2}^{+L_y/2} \left[\left. \frac{\partial \phi}{\partial x} \right|_{z=0} \right]^2 dy \\
&= (U_\infty/g)^2 \, \dot{\boldsymbol{\phi}}^T \cdot \mathbf{M}_{\mathrm{free}} \, \dot{\boldsymbol{\phi}}
\end{aligned} \tag{31}$$

Replacing this expressions in (16):

$$G(x) = {}^1\!/_2 \rho \left[\dot{\boldsymbol{\phi}}^T \cdot \tilde{\mathbf{M}} \, \dot{\boldsymbol{\phi}} - \boldsymbol{\phi} \cdot \mathbf{K} \boldsymbol{\phi} \right] \tag{32}$$

Now we compute $G(x_{\mathrm{out}})$ by replacing $\boldsymbol{\phi}$ for the downstream far-field expansion in (32). Taking account of the orthogonality between the eigenvectors (22),

we arrive to:

$$\begin{aligned}
\boldsymbol{\phi}^T \cdot \mathbf{K}\, \boldsymbol{\phi} &= -\sum_{k=1}^{N_{\text{inv}}} |\lambda_k|\, b_k^2\, \sin^2(\mu_k x + \gamma_k)\, (\boldsymbol{\phi}_k^T \bar{\mathbf{M}} \boldsymbol{\phi}_k) \\
&\quad + \sum_{k=N_{\text{inv}}+1}^{N_{\text{slab}}} \lambda_k (a_k^-)^2 e^{-2\mu_k x} (\boldsymbol{\phi}_k^T \cdot \bar{\mathbf{M}} \boldsymbol{\phi}_k) \\
\dot{\boldsymbol{\phi}}^T \cdot \bar{\mathbf{M}}\, \dot{\boldsymbol{\phi}} &= \sum_{k=1}^{N_{\text{inv}}} |\lambda_k|\, b_k^2\, \cos^2(\mu_k x + \gamma_k)\, (\boldsymbol{\phi}_k^T \bar{\mathbf{M}} \boldsymbol{\phi}_k) \\
&\quad + \sum_{k=N_{\text{inv}}+1}^{N_{\text{slab}}} \lambda_k (a_k^-)^2 e^{-2\mu_k x} (\boldsymbol{\phi}_k^T \cdot \bar{\mathbf{M}} \boldsymbol{\phi}_k)
\end{aligned} \tag{33}$$

and then;

$$\begin{aligned}
G(x) &= \tfrac{1}{2}\rho \sum_{k=1}^{N_{\text{inv}}} |\lambda_k|\, b_k^2\, (\boldsymbol{\phi}_k^T \cdot \bar{\mathbf{M}} \boldsymbol{\phi}_k) \\
&= -\tfrac{1}{2}\rho \sum_{k=1}^{N_{\text{inv}}} b_k^2\, (\boldsymbol{\phi}_k^T \cdot \mathbf{K} \boldsymbol{\phi}_k), \quad \text{para } x > L
\end{aligned} \tag{34.a,b}$$

As expected, this quantity is independent of x. The same procedure can be applied to $x < -L$ and, as the amplitude of the inviscid modes is null there:

$$G(x) = 0, \quad \text{for } x < -L \tag{35}$$

Now replacing in (11):

$$F_x = \tfrac{1}{2}\rho \sum_{k=1}^{N_{\text{inv}}} b_k^2\, (\boldsymbol{\phi}_k^T \cdot \mathbf{K} \boldsymbol{\phi}_k) \tag{36}$$

Note that this expression guarantees always a non-negative wave resistance.

Practical implementation of (36) involves transforming the potential vector for several layers (two are enough) near the outlet plane to the **U** basis. The transformation matrix **S** has been already computed in order to compute the DNL absorbing boundary condition. For each inviscid mode k the amplitude is computed at both layers $U_k(x_{j-1})$ and $U_k(x_j)$ and the amplitude and phase b_k, γ_k can be easily obtained. Off course, the phase is irrelevant to the calculation of drag.

5. Numerical examples

Several numerical examples will show that the proposed strategy gives always positive resistances and very well defined peaks in the drag curve. We present two 2D examples with analytical solution and two 3D examples. Three of the examples do not include ship forms, and are based on a related problem where the wave pattern is produced by a local change in atmospheric pressure by a device like an hover-craft. The advantage of this kind of problem is that it has an analytical solution.

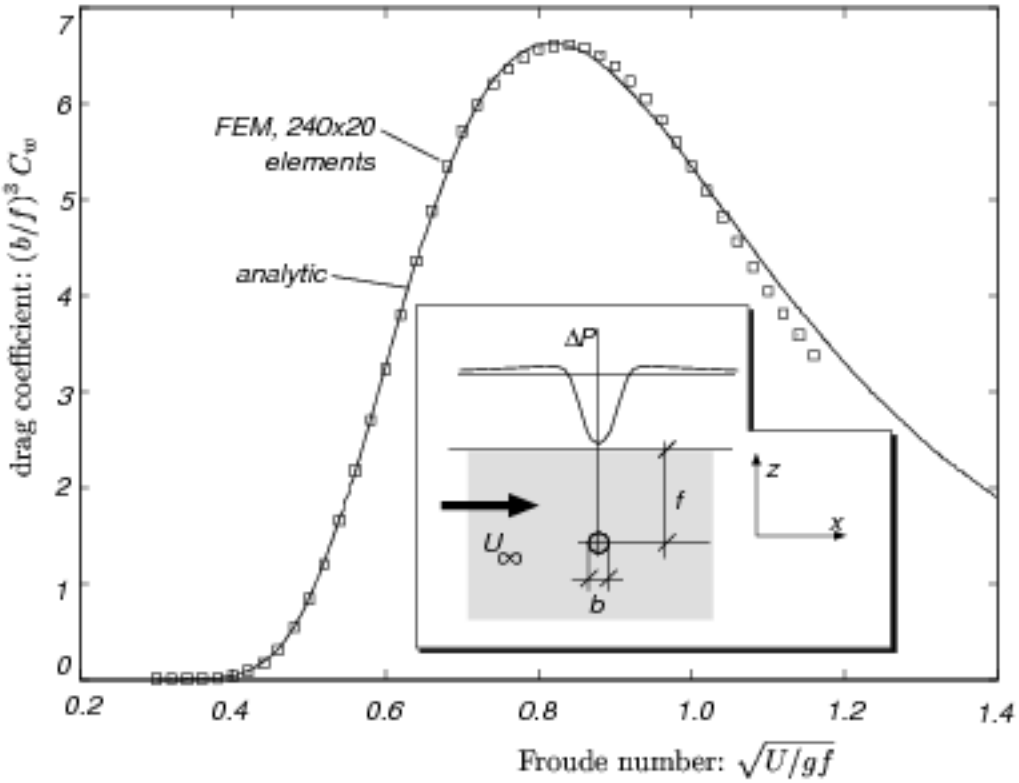

Figure 5: Drag curve for the submerged dipole (cylinder with diameter $b \ll f$). The drag coefficient is normalized to $b/f = 1$. (File: d(pole))

5.1. Submerged dipole: A submerged dipole can be thought as the limit of a cylinder of vanishing radius. The problem was solved by replacing the dipole by a perturbation in the atmospheric pressure, i.e. as an *"equivalent hover-craft problem"*. The drag coefficient can be computed in closed form and is:

$$C_w = \frac{F_x}{\rho {U_\infty}^2 b} = 4\pi^2 (b/f)^3 \, \mathrm{Fr}^{-6} \, e^{-2/\mathrm{Fr}^2} \tag{37}$$

where $f = 1$ is the depth, b the radius of the cylinder (we assume $b/f \ll 1$), and $\mathrm{Fr} = U_\infty/\sqrt{gf}$, the Froude number based on depth. The FEM mesh was structured, with $2 \times 240(x) \times 20(z)$ triangular elements covering the rectangle $|x| < 6$, $-3 < z < 0$. The mesh was refined near the surface in such a way that $\Delta z_{\mathrm{bottom}}/\Delta z_{\mathrm{surface}} = 10$. Note that b enters only through the intensity of the equivalent dipole, so that we plot $(b/f)^3 C_w$, which is a quantity depending only on the Froude number.

5.2. Parabolic pressure distribution: This is another $2D$ example, with a prescribed pressure distribution of the form:

$$\Delta P = \begin{cases} 1 - (x/a)^2; & \text{para } |x| < a; \\ 0; & \text{para } |x| > a; \end{cases} \tag{38}$$

The analytical drag coefficient is:

$$C_w = \frac{F_x}{\rho {U_\infty}^2 a} = 16 \frac{(Ka \cos Ka - \sin Ka)^2}{(Ka)^3} \tag{39}$$

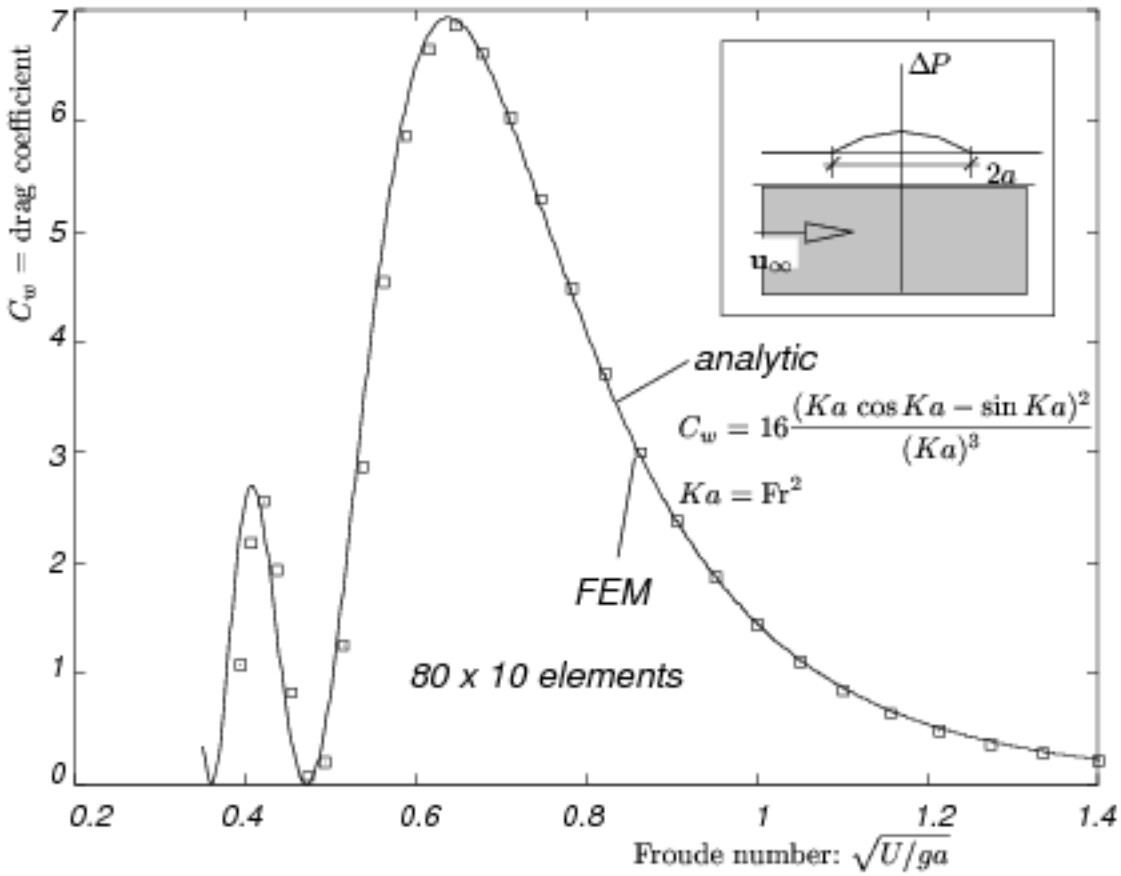

Figure 6: Drag curve for the parabolic pressure distribution. (Fig: bump)

where $Ka = 1/\mathrm{Fr}^2 = ga/{U_\infty}^2$, and the Fr number is taken based on a. The mesh had $2 \times 80 \times 10$ triangular elements with $\Delta x = \text{cte}$ and $\Delta z_{\text{bottom}}/\Delta z_{\text{surface}} = 10$, covering the region $-6 < x < 2$, $-3 < z < 0$.

5.3. Wigley hull: The drag curve for the Wigley model 1805 A is shown in figure 7. The hull shape for this model is defined by $y = \pm(1 - x^2/64)(1 - 0.6x^2/64)(1 - z^2)$ for $|x| < 8$, $z > -1$. The *"circular Froude coefficient"*[7] is defined as:

$$C_w = \frac{250}{\pi} \frac{F_x}{\Omega_{\text{ship}}^{2/3} \rho {U_\infty}^2} \tag{40}$$

where $\Omega_{\text{ship}} = 4\,{}^{52}/_{75}$ is the volume of the ship. The FEM mesh had $50(x) \times 13(y) \times 13(z) = 8450$ elements, and the results are in good agreements with those found in the literature[2,7]. No analytical solutions are available in this case (the continuous curve in the small plot at low Froude numbers simply fits the FEM results). Note that a whole set of secondary maxima is cleanly captured, extending to Froude as low as 0.1. In the other extreme, Froude numbers as high as 1.2 are computed without problems, whereas standard methods like those derived from Dawson suffer from reflections specially at high Froude numbers.

5.4. Rectangular pressure distribution: We consider a uniform rectangular pressure distribution of width B and length L, such that $L/B = 3/2$, for which experimental and analytical results are reported in Wehausen's review[7]. No ana-

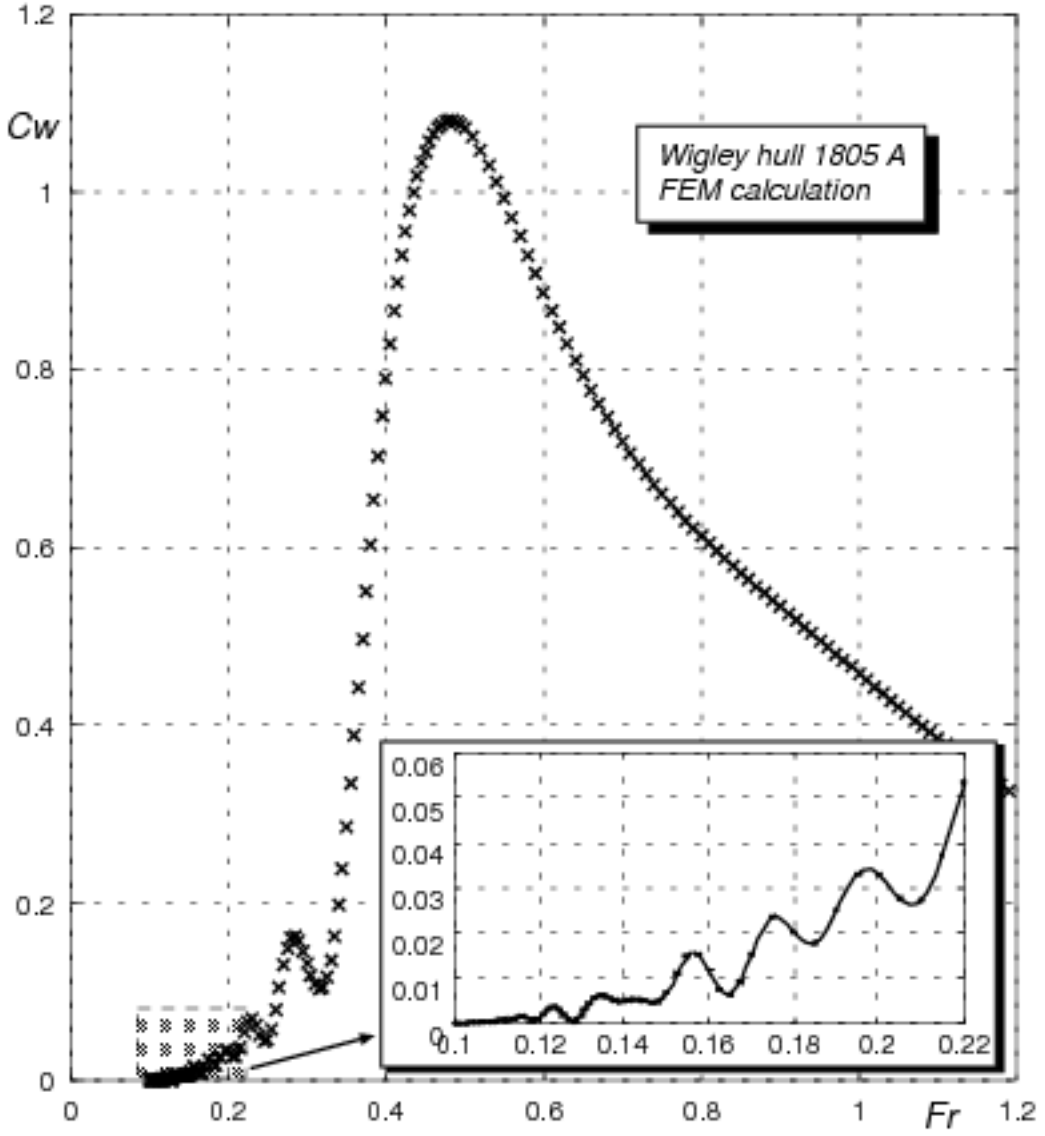

Figure 7: Drag curve for the Wigley hull. The continuous curve in the (Flux wigley)

lytical solutions are shown in this case (the continuous curve simply fits the FEM results). This case is interesting, since it is purely 3D and large oscillations in the drag curve at small Froude numbers are expected, due to the discontinuity in the pressure distribution. The mesh had $30(x) \times 15(y) \times 10(z) = 4500$ elements. Coincidence with results reported in Wehausen's review are very good. Whereas only the maximum around $\mathrm{Fr} = 0.33$ is shown in those results, we arrive here to capture two additional maxima at $\mathrm{Fr} = 0.215$ and 0.255, approximately.

6. Conclusions

We presented a method that allows computation of the wave resistance by integration of the momentum flux at the outlet plane instead of the traditional pressure integration over the hull. A key point in this development is the use of a centered method (i.e., without numerical viscosities) for the discretization of the free surface operator, since this would represent a lost of momentum. Computed

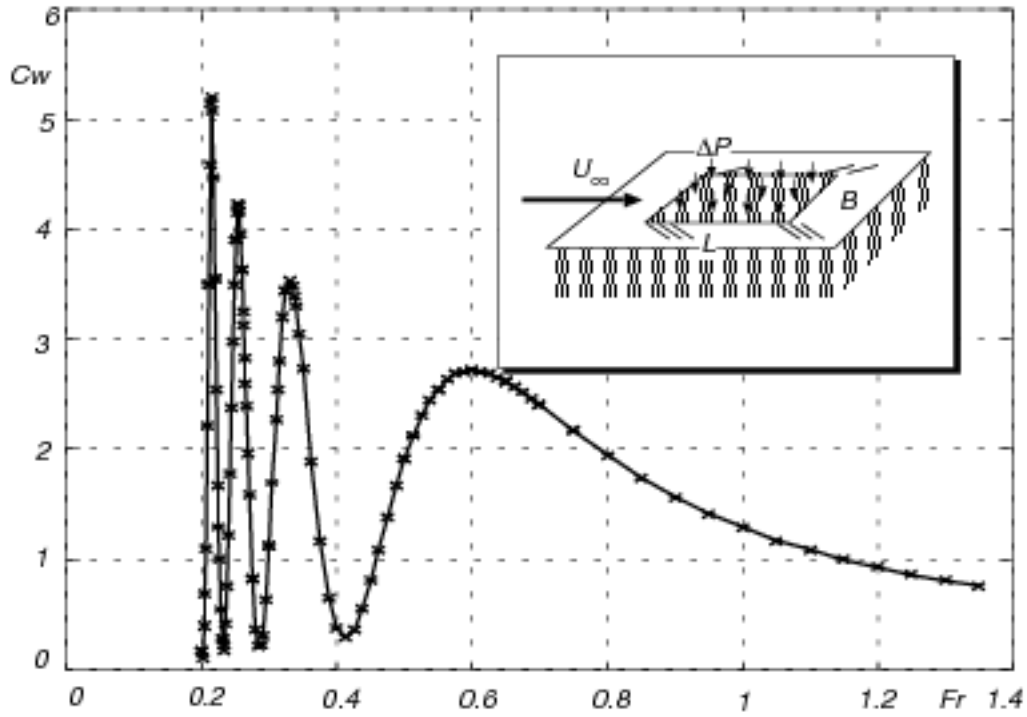

Figure 8: Drag curve for the rectangular pressure distribution.(File: square)

drag curves show very clean peaks, notably at low Froude numbers, and drags are always non-negative.

7. Acknowledgments

This work has received financial support from *Consejo Nacional de Investigaciones Científicas y Técnicas* (CONICET, Argentina) through grant BID 802/OC-AR PID Nr. 26, and from *Universidad Nacional del Litoral* (Argentina), and was done in collaboration with CIMNE (*Centro Internacional de Métodos Numéricos en Ingeniería*, Barcelona). We made extensive use of software distributed by the *Free Software Foundation / GNU-Project*: Linux ELF-OS, Octave, Tgif, Fortran f2c compiler, and others.

8. References

1. M. Storti, J. D'Élía and S. Idelsohn, "Algebraic Discrete Non-Local (DNL) Absorbing Boundary Condition for the Ship Wave Resistance Problem", to appear in Journal of Computational Physics , (1997)
2. Dawson C.W., "A Practical Computer Method for Solving Ship-Wave Problems", in Proceedings 2nd International Conference on Numerical Ships Hydrodynamics, Berkeley, C.A., p.30 (1977).
3. J. Broeze and J.E. Romate, "Absorbing Boundary Conditions for Free Surface Wave Simulations with a Panel Method", Journal of Computational Physics **99**, pp. 146 (1992)
4. Raven H.C., "A Solution Method for the Nonlinear Ship Wave Resistance Problem", Thesis Doctoral, Maritime Research Institute Netherlands (MARIN), (1995).
5. Storti M., "Implementation details of the absorbing boundary

condition for the ship wave-resistance problem. Computing the drag from the wave amplitude", GTM Internal Report. (in Spanish, ftp://galileo.unl.edu.ar/pub/mstorti/wdrag10.ps.gz)
6. J. D'Elia, "Numerical Methods for the Ship Wave-Resistance Problem", Ph.D. thesis, Univ. Nacional del Litoral (Santa Fe, Argentina) (1997)
7. Wehausen J.V., "The Wave Resistance of Ships", Advances in Applied Mechanics, vol 13, pp. 93-245 (1973).
8. S. Ohring, "Three-Dimensional Ship Wave Generation Using an Efficient Finite Difference Scheme with Double Model Linearization", Journal of Computational Physics **41**, pp. 89-114 (1981)
9. Y. Tahara, F. Stern and B. Rosen, "An Interactive Approach for Calculating Ship Boundary Layers and Wakes for Nonzero Froude Number", Journal of Computational Physics **98**, pp. 33-53 (1992)
10. J. Farmer, L. Martinelli and A. Jameson, "Fast Multigrid Method for Solving Incompressible Hydrodynamic Problems with Free Surface", AIAA Journal **32**, p. 1175 (1994)
11. C. Baumann, M. Storti and S. Idelsohn, "A Petrov-Galerkin Technique for the solution of transonic and supersonic flows", Computer Methods in Applied Mechanics and Engineering , **95**, pp. 49-70 (1992)
12. M. Storti, N. Nigro and S. Idelsohn "Equal-Order Interpolations: A Unified Approach to Stabilize the Incompressible and Convective Effects", Computer Methods in Applied Mechanics and Engineering , **143** No 3-4, pp. 317-331 (1997)
13. N. Nigro, M. Storti and S. Idelsohn, "Fluid flows around turbomachinery using an explicit seudo-temporal Euler FEM code", Communications in Numerical Methods in Engineering **11**, pp. 199-211, (1995)
14. Givoli D. and Keller J.B., "Non-reflecting boundary conditions for elastic waves", Wave Motion **12**, pp. 261-279 (1990)
15. Hagstrom T. and Keller, H.B. "Exact boundary Conditions at an Artificial Boundary for partial Differential Equations in Cylinders", SIAM J. Math. Anal. **17**, pp. 322-341, (1986).
16. Hagstrom T. "Boundary Conditions at Outflow for a Problem with Transport and Diffusion", Journal of Computational Physics **69**, pp. 69-80, (1987).
17. Lenoir, M. and Tounsi, A.; "The Localized Finite Element method and its Application to the Two-Dimensional Sea-Keeping Problem", SIAM J. Numer. Anal. **25**, pp. 729-752, (1988).
18. Givoli, D., "Non-reflecting Boundary Conditions", Journal of Computational Physics **94**, pp. 1-29, (1991).
19. Givoli, D., and Keller, J.B.; "A Finite Element Method for Large Domains", Computer Methods in Applied Mechanics and Engineering **76**, pp. 41-66, (1989).
20. Givoli, D., Patlashenko, I. and Keller, J.B. "High-order boundary conditions and finite elements for infinite domains", Computer Methods in Applied Mechanics and Engineering , **143**, page 13-39, (1997)
21. I. Patlashenko and D. Givoli, "Non-local and Local Artificial Boundary

Conditions for Two-Dimensional Flow in an Infinite Channel", International for Journal Numerical Methods in Heat and Fluid Flow , **6**, pp. 47-62, (1996)